

©Copyright 2023

Aparajit Venkatesh

# A Novel Algorithm to Detect and Prevent Slip During Dynamic Object Manipulation Using Tactile Feedback

Aparajit Venkatesh

A thesis  
submitted in partial fulfillment of the  
requirements for the degree of

Master of Science

University of Washington

2023

Reading Committee:

Xu Chen, Chair

Santosh Devasia

Joshua Smith

Program Authorized to Offer Degree:  
Department of Mechanical Engineering

University of Washington

**Abstract**

A Novel Algorithm to Detect and Prevent Slip During Dynamic Object Manipulation  
Using Tactile Feedback

Aparajit Venkatesh

Chair of the Supervisory Committee:  
Xu Chen

Robotic object manipulation has increased exponentially over the last couple of decades across the field of manufacturing, medical robotics, assistive care and warehousing. Detection and prevention of slip of objects plays a vital role in secure object grasping and manipulation. Through the sensory feedback provided by their skin, humans possess the remarkable ability to readily perceive slip. In order to attain a level of skill comparable to humans, robots must be equipped with artificial tactile sensing integrated into their system. In our work, we use an optical tactile sensor, GelSight sensor for real time tactile feedback. We decompose the problem of slip detection as a classification problem by using the input from the GelSight sensor as features. Once slip is detected appropriate corrective actuation is taken to prevent slip. Through this approach we are able to achieve an accuracy of 99% for slip detection for an assortment of objects of different sizes, shapes, textures and rigidity. We then shift gears, and study how slip can be prevented once it is detected. We develop a simplistic and then a more robust algorithm incorporating tactile feedback to detect and prevent slip during dynamic manipulation tasks at different speeds of manipulation. Finally we discuss the drawbacks of the current approach and how these can be addressed in the future work.

## TABLE OF CONTENTS

	Page
List of Figures . . . . .	iii
List of Tables . . . . .	v
Chapter 1: Introduction . . . . .	1
1.1 Background and Motivation . . . . .	1
1.2 Literature Review and Related Work . . . . .	4
Chapter 2: System Architecture and Methods . . . . .	7
2.1 Robot Setup and System Architecture . . . . .	7
2.2 Object Localization . . . . .	9
2.3 Grasping, Slip Monitoring and Grasp Adjustment . . . . .	12
Chapter 3: Slip Monitoring and Grasp Adjustment . . . . .	13
3.1 GelSight Sensor . . . . .	13
3.2 Translating Images to Features . . . . .	13
3.3 Data Acquisition . . . . .	17
3.4 Classification Method . . . . .	17
Chapter 4: Experiment Results . . . . .	19
4.1 Slip Detection . . . . .	19
Chapter 5: Conclusion and Future Work . . . . .	32
5.1 Conclusion . . . . .	32
5.2 Future Work . . . . .	32
Bibliography . . . . .	35
Appendix A: Training and Testing Data . . . . .	39

Appendix B:	Additional Plots with $V_x$ and Commanded Gripper Position for Different Manipulation Speeds . . . . .	40
-------------	--	----

## LIST OF FIGURES

Figure Number		Page
1.1	The setups employed for the experiments: An UR5e robot arm, a hand Robotiq parallel gripper, the fingertips were replaced by customized metallic adapter equipped with two Gelsight tactile sensors. An Intel real sense depth camera D435i is mounted on the top of the gripper . . . . .	3
2.1	Hardware setup depicting the UR5e with the eye-in-hand Intel RealSense D435i camera and custom metallic grippers with GelSight sensors. . . . .	7
2.2	Robot System Architecture . . . . .	9
2.3	Image feed during localization coordinate acquisition for the object to be grasped. . . . .	11
3.1	Gripper grasping a T-handle hex key, the left image below shows the 3D reconstruction of the tool surface, and the right image below draws the arrows to indicate the displacement of marker dots. . . . .	14
3.2	The displacement of individual markers overlaid on the tactile image, providing an estimation of the shear force field. The translational slip in the Y-direction is illustrated in Figure 4(a), while Figure 4(b) portrays the translational slip in the X-direction. Additionally, Figure 4(c) demonstrates the rotational slip, along with a definition of the x and y-directional displacement. . . . .	15
3.3	A slip trial was conducted to illustrate the change of entropy from the no contact to object, through the initial grasp, to the incipient slip, and ultimately to the loss of contact to object . . . . .	16
4.1	Performance of the developed slip detection for objects with different materials and surface characteristics . . . . .	20

4.2	A demonstration of sliding a book out of a shelf is presented, consisting of multiple stages of grasping. The initial row of images portrays the progressive grasping stages, commencing from (1) static initial grasp, advancing towards (2) an incipient slip at the start of manipulation, further to (3) an actual slip, and culminating at (4) a stable grasp. The subsequent row exhibits the data obtained from a tactile sensor and the corresponding real-time detection of slip. The third row displays the command gripper distance to forestall slippage, whereas the fourth row depicts the entropy and the rate of its alteration throughout the grasping procedure. . . . .	23
4.3	Slip Distance before grasp Stabilization vs Manipulation Speed . . . . .	24
4.4	Proposed Control Logic: $r$ is the reference value of the feature that is used for controlling the actuation of the gripper, $e$ is the difference the reference and the measured feature value, $y$ is the value of the measured feature using the GelSight sensor, $u$ is the actuation to the gripper which is the change in position between the fingers of the gripper . . . . .	25
4.5	Block diagram showing the flow of logic and control during the manipulation task . . . . .	26
4.6	Position Command with and without Feedback Control: In the figure, the label 1 indicates the start of the manipulation task. Since the book is held with a conservative grasp, as soon as the task starts, the object starts to slip. Label 2 indicates the point where the gripper completely loses contact with the book when the robot does not have proportional feedback. And the label 3 indicates the robot having a stable grasp after proper grasp adjustment has been done using proportional feedback . . . . .	28
4.7	Commanded gripping position at manipulation speeds of 0.05 m/s and 0.1 m/s. 1 and 2 indicate the end of manipulation task when the speed of manipulation is 0.1 m/s and 0.05 m/s . . . . .	29
4.8	Commanded Position and $V_x$ at manipulation speed of 0.05 m/s . . . . .	30
4.9	Commanded Position and $V_x$ at manipulation speed of 0.1 m/s . . . . .	31
B.1	Commanded Position and $V_x$ at manipulation speed of 0.05 m/s . . . . .	40
B.2	Commanded Position and $V_x$ at manipulation speed of 0.1 m/s . . . . .	41
B.3	Commanded Position and $V_x$ at manipulation speed of 0.075 m/s . . . . .	41

## LIST OF TABLES

Table Number		Page
1.1	Timeline of Developments in Robotic Tactile Sensing . . . . .	5
4.1	Metrics of Different Classifiers using only $\bar{V}_x$ and $\bar{V}_y$ . . . . .	20
4.2	Metrics of Different Classifiers using all features . . . . .	20



## ACKNOWLEDGMENTS

I would like to express my sincere appreciation to College of Mechanical Engineering, UW+Amazon Science Hub and Amazon Robotics for their support which made this project possible. I would also like to express my heartfelt gratitude to Dr. Xu Chen for his mentorship and guidance, my committee members Dr. Santosh Devasia and Dr. Joshua Smith for their guidance, Xiaohai Hu for his help and support throughout this project, Guiliang Zheng for his help in designing the custom metallic grippers, all the members of the MACS lab for their valuable inputs. My sincere thanks to Mike Wolf and Paul Birkmeyer for their feedback throughout the project. I would also like to thank my parents for their continued support throughout my academic journey.

## DEDICATION

to my parents,

## Chapter 1

# INTRODUCTION

### *1.1 Background and Motivation*

The exponential scale increase in manufacturing, warehousing, and robotic surgeries has made it nearly essential to employ robots for tasks like pick and place, tool handling, object sorting, and delicate instrument manipulation. Having a stable grasp on the manipulated object significantly influences the outcome of these tasks. Detection and prevention of slip are crucial for effective object manipulation and handling. Presently, the predominant methods rely on visual feedback for grasping and manipulating objects. However, humans possess remarkable proficiency in grasping and manipulating unfamiliar objects by relying on tactile sensing through their skin. Humans can securely grasp and manipulate objects based solely on tactile feedback. To enable robots to achieve a similar level of proficiency, it is necessary to equip them with tactile sensing capabilities.

In 1984, Johansson [21] demonstrated how humans utilize glabrous skin receptors and sensorimotor memory to automatically control precision grip when lifting objects with varying surface textures. These findings highlight the synergistic interplay between tactile feedback and sensorimotor memory in humans, enabling them to anticipate slip and adjust their grip force accordingly. Humans not only use tactile feedback for initial object characterization, but also continuously rely on it to adjust their grasp during a manipulation task. Let's consider a simple example of filling a water bottle at a refill station. Initially, when the bottle is empty, we hold it with less force, but as it fills up, we increase the grasp force to account for the increased weight. This adjustment is done continuously and subconsciously, relying mostly on tactile sensing rather than visual feedback. Enabling robots to dynamically adjust their grasp to account for uncertainties and changes during a task will greatly improve the success rate in complex dynamic tasks.

Most existing methods for robust object manipulation require prior knowledge about

the object, such as its weight, dimensions, surface texture, and dynamic loading. However, in dynamic manipulation tasks where loading and surface contact forces constantly change, robotic manipulators often struggle to maintain a secure grasp, resulting in object slippage. In contrast, humans excel at adapting to dynamic changes and successfully completing intricate manipulation tasks through tactile feedback, even without detailed knowledge about the object being manipulated. Enabling robots to perform complex manipulation tasks under dynamic and changing environmental conditions, without relying on a priori information about the object, has immense practical applications, ranging from industrial automation to surgical robotics.

This research primarily focuses on slip detection and prevention in object manipulation. The objective is to identify parameters that can be used to detect slip based on sensory information obtained from tactile sensors. To achieve this, a physics-inspired data-driven approach will be employed, formulating slip detection as a classification problem. By leveraging the randomness in contact forces just before an object starts to slip, an algorithm will be developed to detect slip with remarkable accuracy of 99%.

Furthermore, this study aims to implement a real-time slip detection and prevention algorithm by integrating tactile sensors into the end-effectors of a UR5e robot. A dynamic manipulation task of sliding a book out from a bookshelf is used to demonstrate the effectiveness of the proposed approach. Importantly, our approach eliminates the need for prior knowledge about the object and grasping conditions, providing a significant advantage in real-world scenarios where such information may be limited or entirely unavailable. We first propose a simplistic algorithm to adjust the grasp when slip is detected during complex dynamic tasks. We then study the effect of manipulation speed on grasp and stabilization, discovering the need for a more intelligent actuation strategy. Subsequently, we present a proportional feedback control law using readings from the tactile sensor to adaptively adjust the grasp strategy based on the manipulation speed of the task. The results from testing show significant improvements in the success rate of completing the manipulation task at speeds that were not previously achievable without a feedback control architecture.

At a time when automation and robotics are penetrating every industry, developing ro-

bust systems that can support high throughput has become imperative. Equipping robots with tactile sensors and integrating tactile sensing and feedback into path planning and task planning will undoubtedly play a vital role in developing robots that are robust and adaptable. This study aims to explore one such avenue in which tactile sensing and tactile feedback are used to perform a task where the system dynamics are constantly changing. The results from this work demonstrate that by integrating tactile sensing into traditional industrial robots, tasks can be performed not only with a higher success rate but also at speeds that were previously unattainable.

The remainder of the document will discuss the literature behind tactile sensing and slip detection, the system architecture, methods, results, experiments, and future work.

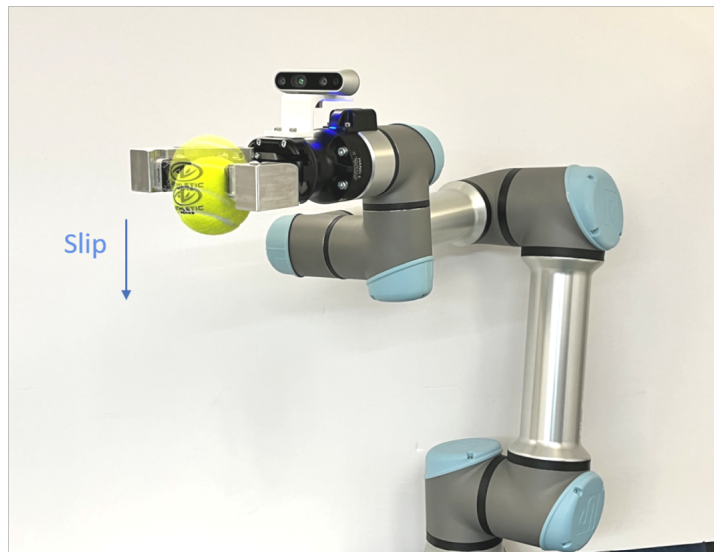


Figure 1.1: The setups employed for the experiments: An UR5e robot arm, a hand Robotiq parallel gripper, the fingertips were replaced by customized metallic adapter equipped with two Gelsight tactile sensors. An Intel real sense depth camera D435i is mounted on the top of the gripper

## 1.2 Literature Review and Related Work

### 1.2.1 Tactile Sensor

With the increasing need for dexterous manipulation, tactile sensing has been growing significantly in the field of robotics. Tactile sensing can be done intrinsically or extrinsically [38]. Intrinsic sensing is done by measuring contact forces through joint torques [5] [33] or through the tension of the transmission cables in manipulators and robotic hands which are equipped with manipulators [20]. The limitation of intrinsic sensing lies in its inability to accurately detect the intricate features of objects. Extrinsic sensors are attached to the exterior of the robotic hand or gripper. An array of piezoelectric sensors can be used to obtain normal force and pressure distribution of the contact surface between the object and the sensor [37]. Multi-modal sensors, such as the BioTac [30], are able to provide the user with various sensory information including force, temperature, vibrations, etc. Nevertheless, in scenarios involving multi-force interactions, piezoelectric and many multi-modal tactile sensors may not offer sufficient high-resolution sensor data. Optics-based tactile sensors [36] have been used to bridge this gap and provide high-resolution 2-D or 3-D images of the surface contour of the objects, through which the surface interaction forces can be inferred. Optical tactile sensors like Tactip [36] and the one developed in [15] provide optical information regarding the minor surface distortions of the contacting surface between the sensor and the object during the interactions which can then be used to infer the contact forces. In addition to this, table 1.1, encapsulates all the work done in the field of tactile sensing through the years.

As we can see, optical tactile sensing is topic that has grown in utility in recent years with the need for robots to perform dexterous tasks. The GelSight sensor is an optical tactile sensor, designed for high-precision measurement of contact surface geometry [42] [14]. It utilizes a clear elastomer coated with a reflective gel. which records surface deformation upon contact with an object. This produces images used to generate a depth map of the contact surface. For our project, we used the commercially available GelSight Mini sensor with marker dots on its cartridge.

Table 1.1: Timeline of Developments in Robotic Tactile Sensing

Year	Development	Importance
1950s-1970s	Initial research on tactile sensors [2]	Laid the foundation for future advancements in robotic tactile sensing
1980s-1990s	Tactile arrays with multiple sensing elements [12]	Enabled more detailed and localized tactile information gathering
1980s-1990s	Flexible and stretchable sensors [11]	Paved the way for conformable and adaptable tactile sensing systems
2000s-2010s	"Skin-like" tactile sensors [32]	Introduced highly sensitive and flexible sensors mimicking human skin
2000s-2010s	Integration of tactile sensors with robotic hands [10]	Enabled robots to perform delicate tasks requiring tactile feedback
2010s-present	Bioinspired tactile sensors [31]	Inspired by natural systems, these sensors enhanced robot perception and interaction capabilities
2010s-present	Integration of MEMS sensors [23]	Miniature MEMS sensors enabled compact and high-resolution tactile sensing systems
2010s-present	Tactile perception and object recognition algorithms [24]	Algorithms improved robot's ability to understand and manipulate objects based on tactile information
2010s-present	Integration of tactile sensing with vision [6]	Combined tactile and visual data for more comprehensive perception in robots
2010s-present	Haptic feedback systems for robots [28]	Enabled robots to provide realistic touch-based feedback to users

### 1.2.2 Slip Detection

The topic of slip detection is not new, and numerous methods have been proposed to address this problem. In 1989, Howe [16] designed a skin acceleration sensor that could detect the slip and texture of a grasped object. In 2004, Ikeda [17] used a camera to detect incipient slip, while in 2012, Maldonado utilized fingertip sensing to detect the shape, material, and slipperiness of an object [27].

Current work on slip detection mainly relies on tactile sensing. In 2015, Veiga [35] used traditional tactile sensors and multiple machine-learning classification algorithms to achieve slip detection with an average accuracy of 75%. Subsequently, they also proposed a finger grip stabilization control approach [34]. In 2018, James [19] used TacTip biomimetic vision-based tactile sensors and support vector machines to achieve slip detection. In their later work in 2021, they extended this approach to a multi-finger robot [18]. Dong [13] proposed an incipient slip detection method in 2018 by computing the difference between the theoretical and detected contact region velocities, achieving an accuracy of 86.25%. In 2019, Li [25] combined visual and tactile information and trained a deep neural network to classify slipperiness. Most recently, Griffa [15] employed Deep Neural Network to obtain the distribution of contact forces, which was subsequently utilized for a classification task. Their proposed approach achieved classification accuracy ranging from 74.40% to 79.01% across five distinct objects. Additionally, Juddy [22] used a soft force sensor to anticipate slipperiness in tasks to grasp deformable objects.

To enhance the precision of slip detection, we use GelSight sensor images and extract entropy as a feature to represent the degree of randomness or disorder in the image, providing a reliable indicator of the presence of slip. Our approach eliminates the need for prior knowledge about the object and grasping conditions, offering a significant advantage in real-world scenarios with limited or unavailable prior knowledge.



## Chapter 2

### SYSTEM ARCHITECTURE AND METHODS

#### 2.1 Robot Setup and System Architecture

For the purpose of this study, a UR5e robot equipped with the Robotiq Hand-E Gripper is utilized. The Robotiq Hand-E Gripper is customized with gripper arms to accommodate the GelSight mini tactile sensor. An Intel RealSense D435i camera is mounted on the robot's sleeve to enable an eye-in-hand configuration. In this study, only one GelSight sensor is employed, while a piezo-electric sensor is attached to the surface of the other GelSight sensor to detect initial contact with an object during grasping. The overall experimental setup is illustrated in Figure 2.1.



Figure 2.1: Hardware setup depicting the UR5e with the eye-in-hand Intel RealSense D435i camera and custom metallic grippers with GelSight sensors.

The task planner leverages information from the Intel RealSense D435i RGB-D camera to calculate the object's position and subsequently determine its pose and coordinates for

the robot to execute the grasp. The robot motion planner employs inverse kinematics to compute a path to the desired pose. Once accomplished, the robot controller receives the joint angles as inputs and dispatches appropriate commands to each of the joint motors to drive the robot to the desired pose. After the robot reaches the desired pose, a command is issued to the gripper to initiate the gripping process. A conservative grasp on the object is established with the assistance of a piezoelectric sensor, which detects when the robot's gripper makes contact with the object being grasped. The command to the Robotiq Hand-E gripper encompasses three parameters: position, speed, and force. All commands are discrete values ranging from 0 to 255. Regarding the position command, 0 corresponds to the fully open position, while 255 corresponds to the fully closed position of the gripper. In terms of the speed command, 0 indicates negligible actuation speed, whereas 255 represents an actuation speed of 70mm/s. The force command does not directly correlate with Newtonian force and is utilized as a step function. A value of 0 signifies a very light grip suitable for deformable objects, whereas values above 0 indicate a progressively tighter grip. The robot always operates at its maximum gripping speed to swiftly attain the commanded position.

Once a stable grasp is achieved, the manipulation task commences. Throughout the manipulation task, continuous output from the GelSight Mini sensor is utilized to monitor the state of the grasp, and subsequent commands are sent to the gripper to maintain grasp stability. The GelSight Mini sensor transmits data at a frequency of 10 Hz. At each time step, the quality of the grasp is evaluated based on the received data, and appropriate actuation is employed. The system architecture of the robotic system is depicted in Figure 2. Arrows directed towards the task planner signify information received from the sensors, while arrows originating from the task planner represent commands sent to the actuators.

Although this work briefly touches upon the vision and motion planning aspects of the project, the primary focus lies in the detection of slip and the stabilization of grip through tactile sensing.

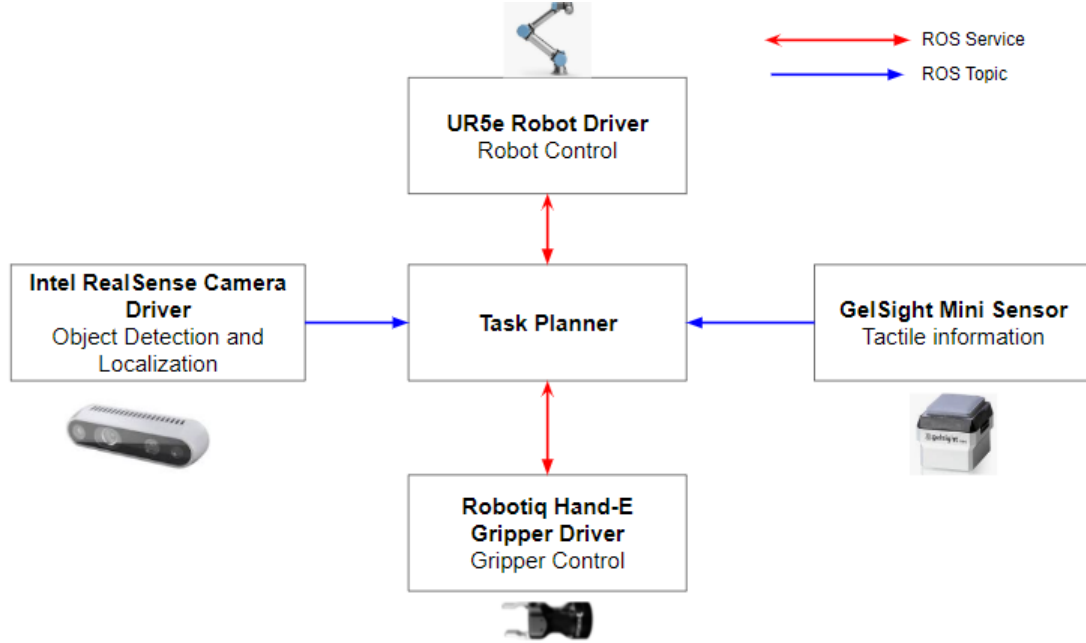


Figure 2.2: Robot System Architecture

## 2.2 Object Localization

Before the robot can grasp the object, the end-effector of the robot needs to be positioned and oriented correctly. An Intel D435i camera is employed to capture the video stream of the environment. The Intel RealSense D435i RGB-D camera utilizes two cameras to estimate stereoscopic depth. It provides RGB images along with depth information. Various methods for object identification and localization can be utilized. In this study, the Scale Invariant Feature Transform (SIFT) algorithm [26] is employed. This algorithm aims to match object features with the live stream of the scene. Once a sufficient number of matching features are found, a bounding box is drawn around the object. Based on the clustering of features, a point on the object is selected in camera coordinates as the grasping point. Intel RealSense provides libraries that include functions for converting 2D pixel camera coordinates to 3D world coordinates. These coordinates are initially defined with respect to the camera, so a translation and rotation transformation is applied to obtain the coordinates with respect to the robot's base. The transformation and rotation

matrix are obtained through a hand-eye calibration process between the camera and the robot's base. This calibration results in a  $4 \times 4$  matrix represented as:

$$\begin{bmatrix} R_{11} & R_{12} & R_{13} & T_x \\ R_{21} & R_{22} & R_{23} & T_y \\ R_{31} & R_{32} & R_{33} & T_z \\ 0 & 0 & 0 & 1 \end{bmatrix} \quad (2.1)$$

The 12 unknown parameters of this matrix are determined through a hand-eye calibration process. Custom printed Aruco markers are utilized as calibration markers. This iterative method employs the Levenberg-Marquardt optimization algorithm. Initially, random parameter assignments are made to the transformation matrix, and the coordinates' reprojected pixels are estimated to determine the pose of the Aruco markers. The reprojection error is then calculated as the sum of squared distances between the extracted feature points and their projections. Finally, the optimization algorithm minimizes this error until it falls below a specified threshold.

Considerable research has been conducted on selecting optimal grasping locations. Methodologies such as Principal Component Analysis, Supervised and Unsupervised learning approaches have been explored. However, this work focuses more on maintaining a stable grasp of an object after the initial grasp has been established. Consequently, the geometric midpoint of the bounding box in pixel coordinates is chosen as the middle point of the X-Y plane of the robot's end-effector.

Once the appropriate coordinate is determined, the end-effector is commanded to move to that target pose. Inverse kinematics is employed to calculate the joint angles for the motion, and this data is subsequently sent to the robot controller, which actuates the motors accordingly to drive the robot to the commanded pose.

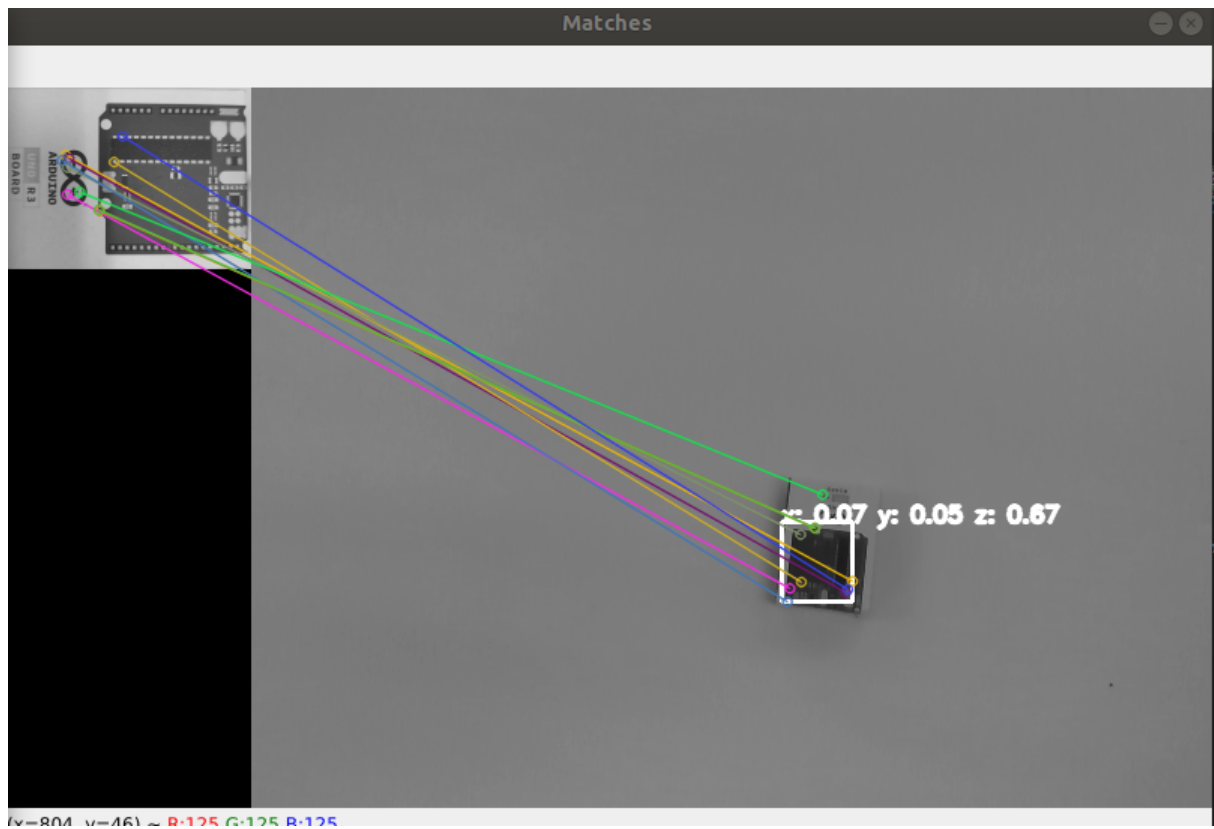


Figure 2.3: Image feed during localization coordinate acquisition for the object to be grasped.

### ***2.3 Grasping, Slip Monitoring and Grasp Adjustment***

The UR5e robot is equipped with a Robotiq Hand-E Gripper, which has modified gripper arms designed to accommodate the GelSight sensor. Once the robot’s end-effector reaches the desired pose, the gripper arms begin closing until the piezo-electric sensor makes contact with the grasped object. The piezoelectric sensor detects this contact and generates a voltage reading, indicating successful contact. It is crucial to employ a conservative grasping strategy when initially grasping objects to avoid damaging them. Therefore, the piezoelectric feedback is utilized to determine when the initial contact has been established, allowing the object to be grasped with the least amount of force. This strategy is particularly valuable when handling deformable objects.

After the initial grasp is achieved, the GelSight sensor is employed throughout the manipulation task to monitor slip in real-time. When slip is detected, the grasp strategy is dynamically adjusted to prevent further slippage. We propose a simple incremental strategy in which the distance between the gripper fingers is incremented by one unit every time slip is detected. For example, if the manipulation task starts with a gripper distance of 160, each slip detection event leads to an increase of one unit, resulting in a reduced distance between the gripper fingers. Subsequently, we investigate the impact of manipulation speed on the effectiveness of this approach. Our findings reveal that at high manipulation speeds, this method fails to adequately stabilize the grasp. To address this issue, a straightforward proportional feedback control logic is implemented and its effectiveness is examined. Section 3 will provide a detailed discussion on the output images obtained from the GelSight sensor and how these outputs are utilized for slip detection.

## Chapter 3

### SLIP MONITORING AND GRASP ADJUSTMENT

#### 3.1 *GelSight Sensor*

The GelSight Mini is optical tactile sensor. It sensor has a soft elastomer as its contact surface. The deformation of the soft elastomer surface is measured using a small Arducam camera. The high resolution 3D and 2D geometries are reconstructed from the camera images. When the sensor surface is painted with black markers, the motion of the markers provide qualitative about the shear forces. Due to the size and dimension of the GelSight Mini it can be easily installed on robotic platforms. The GelSight outputs at rate of 20 frames per second. Figures 3.1 shows the 3D reconstruction of the surface and the qualitative shear force shown by the arrows that are calculated the using the displacement of the marker dots.

#### 3.2 *Translating Images to Features*

In Figure 3(b), a 3-dimensional contour depicting the T-handle hex key's contact with the GelSight sensor is shown. Figure 3(c) displays arrows representing the deformation of the gel that results from contact forces [41], represented by  $Dx_i$  and  $Dy_i$ . In the context of this study, the aforementioned arrows are referred to as the displacement field of the markers.

The magnitude of the arrows is directly proportional to the extent of the local deformation of the gel coat surface. In this study, we propose the utilization of the rate of change of magnitude of the arrows in both the  $x$  and  $y$  directions as characteristic features that can indicate slip. Figure 3.2 illustrates the marker flow exhibiting both translational slip and rotational slip. To quantify the observed features, we define the discrete-time velocity features  $\bar{V}_x$  and  $\bar{V}_y$  as:

$$v_{x_i}(t) = f \cdot (D_{x_i}(t) - D_{x_i}(t - \Delta t)) \quad (3.1)$$

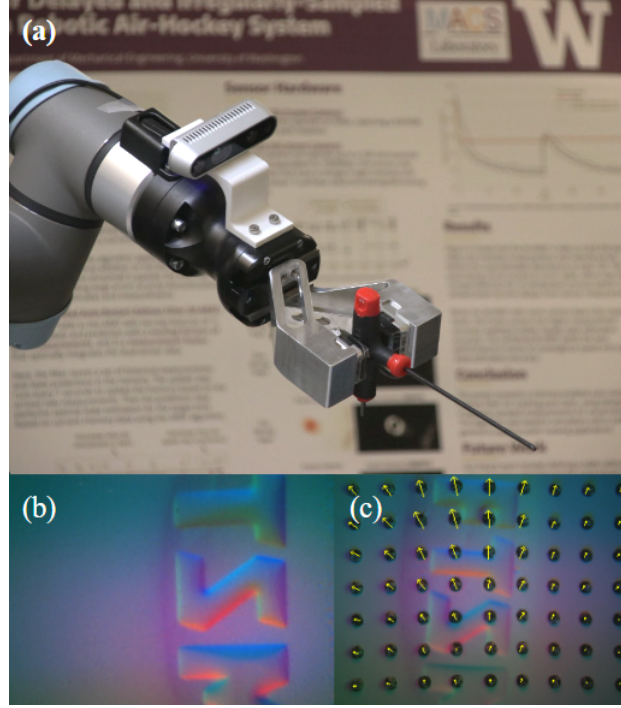


Figure 3.1: Gripper grasping a T-handle hex key, the left image below shows the 3D reconstruction of the tool surface, and the right image below draws the arrows to indicate the displacement of marker dots.

$$\bar{V}_x(t) = \frac{1}{n} \sum_{i=1}^n v_{x_i}(t) \quad (3.2)$$

By the same logic,

$$\bar{V}_y(t) = \frac{1}{n} \sum_{i=1}^n v_{y_i}(t) \quad (3.3)$$

Here,  $f$  is the sampling frequency,  $n$  denotes the total number of data points (in this instance, 63), and  $D_{x_i}(t - \Delta t)$  and  $D_{x_i}(t)$  represent the positions of the  $i$ -th data point at time  $t - \Delta t$  and  $t$ , respectively. By definition,  $v_{x_i}$  and  $v_{y_i}$  refer to the velocity components in the x and y directions of the  $i$ -th data point.  $\bar{V}_x$  is the average velocity in the x-direction,  $\bar{V}_y$  is the average velocity in the y-direction, and  $\Delta t$  is the sampling time, 0.1s in our case since the sampling frequency  $f$  of tactile sensor is 10 Hz. During dynamic manipulation tasks, such as accelerating or altering the course of motion of a robot while securely grasping an object, the magnitudes of marker flow arrows may be altered. This



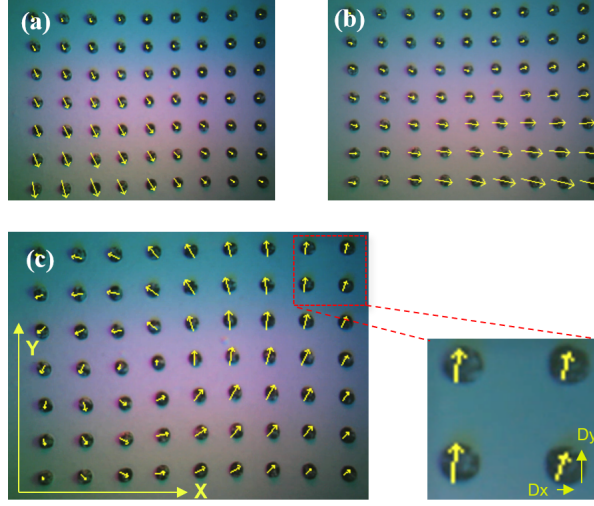


Figure 3.2: The displacement of individual markers overlaid on the tactile image, providing an estimation of the shear force field. The translational slip in the Y-direction is illustrated in Figure 4(a), while Figure 4(b) portrays the translational slip in the X-direction. Additionally, Figure 4(c) demonstrates the rotational slip, along with a definition of the x and y-directional displacement.

presents a challenge in relying solely on the rate of change of magnitudes of the arrows to detect slip, as the changes in magnitude due to acceleration can create false positives. To address this issue, it is necessary to identify distinct features that exclusively indicate slip, thus enabling the construction of a more robust slip detection classifier.

In prior research conducted by Yuan [43], the inhomogeneity of the displacement of marker flow was adopted as a metric to quantify slip. This inhomogeneity is defined as the entropy of marker flow field. Entropy is the statistical measure of randomness of a histogram, expressed as:

$$H(X) = - \int_X p(x) \log p(x) dx \quad (3.4)$$

Here, the histogram  $X$  represents the frequency distribution of the magnitude of the displacement field, and  $p(x)$  denotes the probability density function of the length of the marker flow displacement. When an object begins to slip, the displacement field becomes more erratic due to the non-uniform contact forces that arise throughout the contact surface as the object moves. The inhomogeneity is more significant around the edges of the

contact region, resulting in a non-uniform displacement field and increased entropy, as illustrated in Figure 3.3. Yuan [43] established a correlation between the increase in entropy and the likelihood of incipient occurring. However, solely relying on entropy as a detection metric compresses the valuable information available in the two-dimensional displacement field into a single value, leading to a loss of information. Incorporating entropy as an additional feature into the classification problem would ensure that all available information is utilized. This approach would also eliminate false positives that would arise if only  $\bar{V}_x$  and  $\bar{V}_y$  were used as features. Figure 3.3 shows the plot of the entropy when

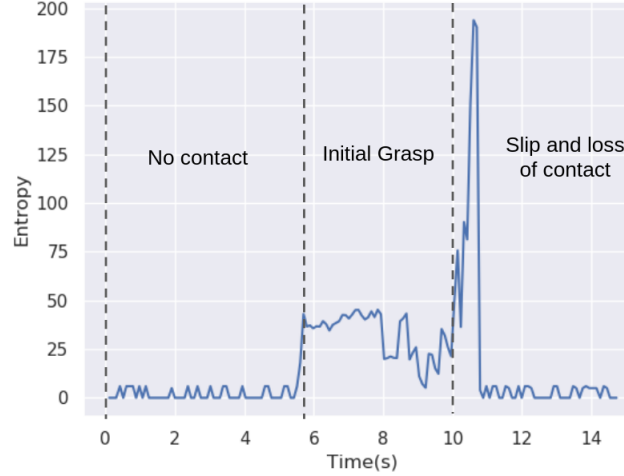


Figure 3.3: A slip trial was conducted to illustrate the change of entropy from the no contact to object, through the initial grasp, to the incipient slip, and ultimately to the loss of contact to object

a grasping action is being performed. It is observed that the entropy increases when the grippers initially come into contact with the object, and this value remains relatively constant as long as the object is securely grasped. However, when the object begins to slip, a sharp increase in entropy is observed. Thus, it is evident that reasonably high entropy values can exist even when an object is securely grasped. Additionally, the entropy remains almost constant when a secure grasp is established. To further enhance the classification of slip, the rate of change of entropy is introduced as another feature to feed into

the classifier. The rate of change of entropy is calculated as follows:

$$\frac{dE(t)}{dt} \approx f \cdot (E(t) - E(t - \Delta t)) \quad (3.5)$$

where  $E$  is the entropy and  $\Delta t$  is the sampling time. The entropy and its rate of change are heavily influenced by the object’s mass and material, making it impractical to establish fixed thresholds. To address this, a range of objects with varying shapes, sizes, weights, and materials were examined to collect the data. Subsequently, this data was utilized to train a classifier, which was capable of categorizing the objects.

### 3.3 Data Acquisition

Our data-driven model requires a smaller amount of labeled data compared to the deep neural network models that have been proposed in the literature. To acquire the necessary data, we selected 10 objects that are commonly encountered on a daily basis. The grasping strategy was adjusted such that the gripper was holding the object with just enough force so as to prevent slip. Once a proper grasping strategy was established, data was collected for one minute for each object. The data set used in this study encompassed all pertinent features, including the mean displacement of the marker flow in the horizontal ( $x$ ) and vertical ( $y$ ) directions, the entropy of the displacement field, and the rate of change of the displacement field’s entropy.

The objects selected for the experiment are depicted in Figure 6. Deformable objects such as sponge scrub were specifically chosen because they have been shown to be difficult to distinguish as slippery in previous work by Dong [13]. The data we collected and used can be accessed at in the link given in Appendix 1.

### 3.4 Classification Method

Four different classification algorithms [9, 7, 8, 4] were adopted for this classification problem:

- Logistic Regression(LR):  $h_{\theta}(x) = \frac{1}{1 + e^{-\theta^T x}}$
- Support Vector Machine (SVM):  $f(x) = \text{sign}(\mathbf{w}^T \mathbf{x} + b)$

- Random Forest (RF):  $f(x) = \frac{1}{T} \sum_{t=1}^T h_t(x)$
- K-Nearest Neighbour (KNN):  $f(x) = \text{mode}(y_i : x_i \in N_k(x))$

Here,  $h_\theta(x)$  represents the probability that the input  $x$  belongs to a certain class,  $\mathbf{w}$  and  $b$  are the weight vector and bias term, respectively, and  $h_t(x)$  denotes the prediction of the  $t$ -th decision tree. The function mode returns the most frequent class label among the  $k$  nearest neighbors of  $x$ .

These algorithms were implemented using the sklearn library in Python. Grid search was performed during training to optimize the hyperparameters for each classification algorithm. The best results were obtained using Logistic Regression with L2 penalty (regularization value of 0.1), KNN classification with nearest neighbor hyperparameter set to 1, and Support Vector Machine Classifier with RBF kernel and regularization parameter of 1. Hyperparameter adjustments did not improve the performance of the Random Forest classifier, so the default hyperparameters were used. A 80-20 split was used for training and testing of data.

## Chapter 4

### EXPERIMENT RESULTS

#### 4.1 Slip Detection

As previously mentioned, four distinct classification algorithms were utilized to detect slips, and each algorithm was assessed using multiple statistic metrics. Furthermore, during the training phase of each model, two separate sets of features were employed. The first set of features contained solely  $\bar{V}_x$  and  $\bar{V}_y$ , while the second set of features incorporated  $\bar{V}_x$ ,  $\bar{V}_y$ , and the newly proposed features: entropy, and the rate of change of entropy. A total of 14,426 data points were utilized during the training process. The performance of the classifier using the collected data is presented in Tables 4.1 and 4.2. In the tables, “Accuracy” represents the percentage of correctly classified instances over the total number of instances; “Precision” is the metric to characterize how well a classifier is able to distinguish a true positive from a false positive. Ideally, both precision and accuracy should be 1 for a perfect classifier. “Recall” characterizes how well a classifier is able to differentiate between true positives and false negatives. The F1 score, which is the harmonic mean of precision and recall, provides a balanced measure of model performance. The results indicate that the random forest classifier consistently outperforms other methods, regardless of the hyper-parameters selected by each algorithms. Moreover, leveraging the proposed inhomogeneity of the arrow displacements and the rate of entropy changes significantly improves the accuracy of most methods. Notably, the accuracy of using the logistic regression algorithm significantly increases from 52.25% to 87.60%. The performance of our slip detector on different objects is illustrated in Figure 4.1. The evaluation is conducted using the Random forest algorithm, and the F1 scores and the recall rates are computed based on the macro average metric. Notably, our classifier performs well on objects with a spherical shape, such as a tennis ball [35]. Moreover, for objects that are prone to deformation [13], our classifier achieves favorable outcomes. The accuracy of slip

classification for all the objects in our experiment is extremely high as indicated by Figure 4.1.

Classifier	Accuracy%	Precision%	Recall%	F1 Score%
LR	52.25	100	2.32	4.54
SVM	94.42	100	88.59	93.95
KNN	96.72	99.34	93.93	96.55
RF	96.83	96.83	94.66	96.69

Table 4.1: Metrics of Different Classifiers using only  $\bar{V}_x$  and  $\bar{V}_y$

Classifier	Accuracy%	Precision%	Recall%	F1 Score%
LR	87.60	92.83	80.88	79.52
SVM	90.26	98.89	80.98	89.85
KNN	97.61	99.88	95.23	97.50
RF	99.14	99.14	98.80	99.11

Table 4.2: Metrics of Different Classifiers using all features











										
Macro Avg:	Screw driver	Tennis ball	Contact Solution	Mouse	Box	Highlighter	Toy Raccoon	Sponge	Toy Owl	Floss
Accuracy	99.63%	100%	100%	99.74%	99.35%	99.73%	99.35%	100%	99.44%	97.59%
Recall	99.60%	100%	100%	99.57%	99.35%	99.67%	99.34%	100%	99.34%	98.07%
F1 Score	99.61%	100%	100%	99.66%	99.35%	99.70%	99.34%	100%	99.38%	97.82%

Figure 4.1: Performance of the developed slip detection for objects with different materials and surface characteristics

To evaluate the efficacy of the developed classifier during dynamic tasks, we designed a robotic-grasping experiment, which is discussed in the next section.

#### 4.1.1 *Dynamic Manipulation Task: Sliding a book out from a shelf*

In this experiment, a UR5e robot is employed to execute a task involving the retrieval of a book from a shelf and sliding it to a new position. As prior information regarding the weight and stiffness of the object was not available, the implementation of a cautious grasp strategy, characterized by a relatively diminished clamping force, is deemed necessary in order to forestall any potential damage. The experimental procedure started with positioning the parallel gripper adjacent to the bookshelf without making initial contact with the book. The gripper was then maneuvered towards the book, and a safe grasp was executed using appropriate parameters, which entailed a relatively low grasping force. No slip occurred during the pre-manipulation phase. However, during the subsequent stage of extracting the book, the absence of a slip detection method and corresponding prevention algorithm resulted in the book slipping, thus interfering with the successful completion of the manipulation task.

To overcome this issue, the experiment was replicated with the incorporation of the proposed slip detection algorithm and a subsequent slip-prevention force control of the gripper in the robotic system. The detection algorithm successfully identified the initial slip when the robot attempted to extract the book. Despite the gradual increase in grasping force, the smooth book cover and the drag exerted by the gripper caused the incipient slip to increase. The slip-prevention algorithm responded by gradually increasing the grasping force until a stable grasp was achieved, which was maintained for a brief duration to ensure secure gripping of the book. While maintaining the grasping force, the robot slid the book out of the bookshelf and adjusted the force as necessary to prevent further slips. After the book is extracted, the grasping force is gradually reduced to release the book. With the slip detection and prevention algorithms implemented, the grasp was continuously sustained, and the manipulation task was accomplished successfully using the same set of initial grasping parameters.

The grasping stages during the book extraction task and their corresponding entropy and rate of change of entropy are denoted as (1)-(4), illustrated in Figure 4.2. The figure indicates that the entropy and the rate of change of entropy are almost negligible when the

book is held with safe grasping parameters. However, as the manipulation process begins, the entropy and the rate of change of entropy slightly increase, indicating the need for a grip adjustment. As the manipulation process proceeds, the entropy and the rate of change of entropy continue to increase, indicating the occurrence of more slip. To prevent slip, the gripping pose is further modified until the entropy reaches a constant value and the rate of change of entropy approaches zero. It is noteworthy that the entropy value is higher at the end of the manipulation process than that at the start, which can be attributed to the dynamic forces acting on the book during the manipulation process, resulting in non-homogeneity in the marker field. Even though a firm grip is established at the end of the manipulation process, the non-homogeneity in the marker field remains. In conclusion, the changes in entropy and the rate of change of entropy during the book extraction task provide valuable insights into the manipulation process and the effectiveness of slip detection techniques. The experiment shows that slip detection can effectively prevent slip and enable successful manipulation tasks, as evidenced by the adjustments made to the grip during the book extraction task.



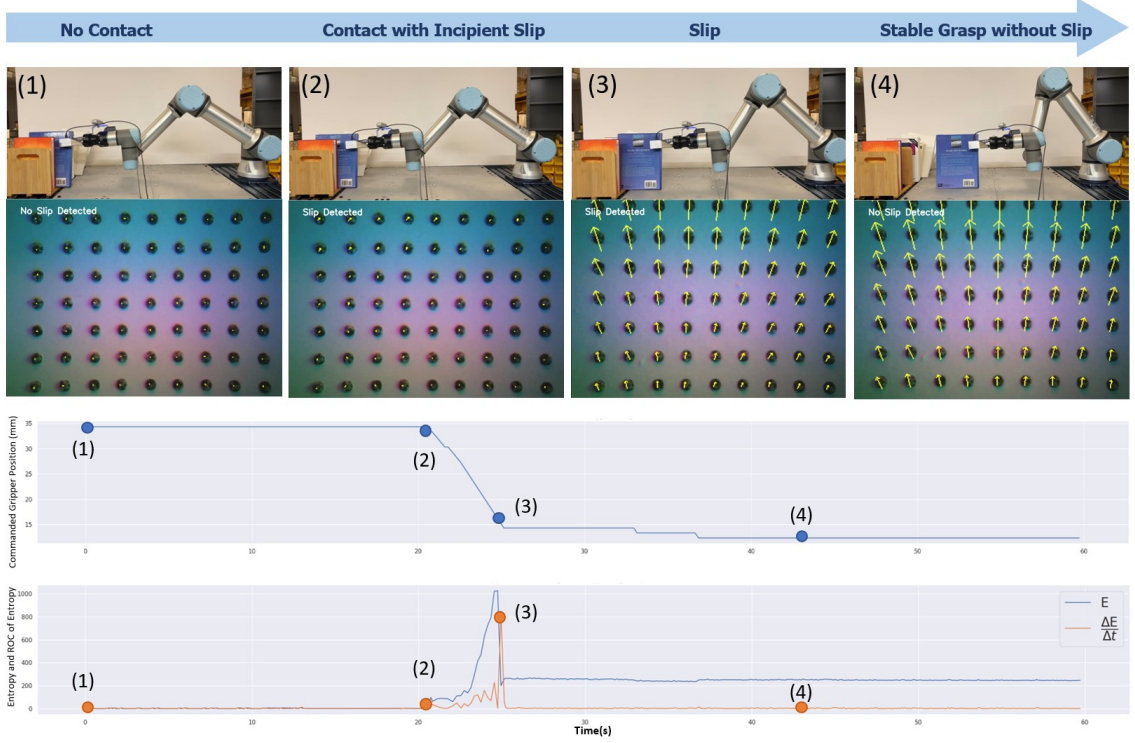


Figure 4.2: A demonstration of sliding a book out of a shelf is presented, consisting of multiple stages of grasping. The initial row of images portrays the progressive grasping stages, commencing from (1) static initial grasp, advancing towards (2) an incipient slip at the start of manipulation, further to (3) an actual slip, and culminating at (4) a stable grasp. The subsequent row exhibits the data obtained from a tactile sensor and the corresponding real-time detection of slip. The third row displays the command gripper distance to forestall slippage, whereas the fourth row depicts the entropy and the rate of its alteration throughout the grasping procedure.

#### 4.1.2 Intelligent Control using Tactile Feedback

Although the method described in the previous section achieved success in the specified manipulation task, it exhibited limitations when the manipulation speed was altered. In the implemented algorithm, the gripping distance between the fingers was incrementally reduced upon slip detection. However, this incremental reduction remained constant regardless of the manipulation speed, as the actuation speed was always set to its maximum value. To further investigate the impact of manipulation speed on the grasp stabilization,

the same experiment as detailed in the previous section was conducted at various manipulation speeds. This experiment aimed to measure the distance by which the book slipped before the grasp was successfully stabilized. The results of this experiment are depicted in Figure 4.3.

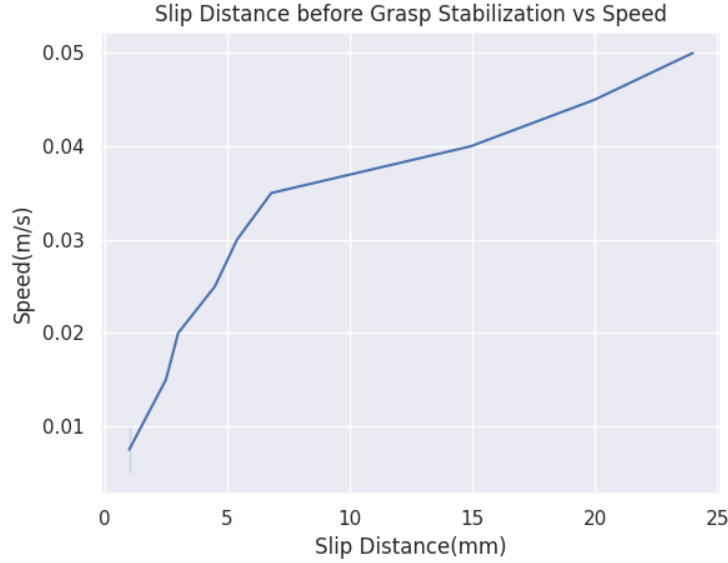


Figure 4.3: Slip Distance before grasp Stabilization vs Manipulation Speed

We observe from the graph that maintaining the same actuation while varying manipulation speeds leads to a significant increase in the distance the book slips. Specifically, when the speed is increased to 10 times the initial value, the distance required for grasp stabilization is amplified by a factor of 25. Although the manipulation task succeeded in stabilizing the grasp for the book, which had sufficient surface area to hold onto after slipping, objects with inadequate surface area would likely result in task failure.

Hence, there is a necessity to develop a more sophisticated control algorithm that surpasses constant incremental actuation. Figure 4.4 illustrates a proposed control logic:

When developing a control logic, it is crucial to select appropriate reference values for the desired signals. Intuitively, the reference values for  $V_x$  and  $V_y$  can be derived, as they represent the velocity components in the x and y directions, respectively. However, deter-

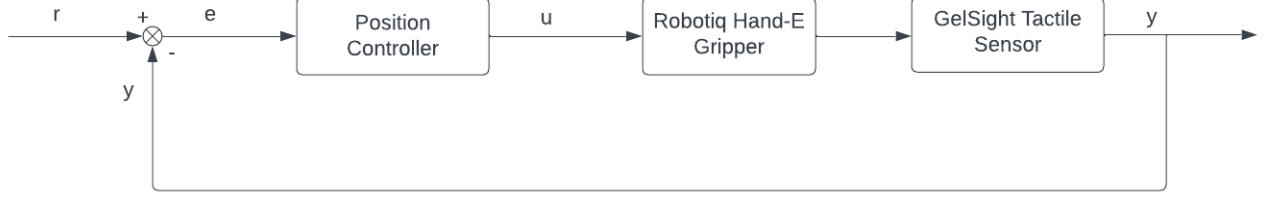


Figure 4.4: Proposed Control Logic:  $r$  is the reference value of the feature that is used for controlling the actuation of the gripper,  $e$  is the difference the reference and the measured feature value,  $y$  is the value of the measured feature using the GelSight sensor,  $u$  is the actuation to the gripper which is the change in position between the fingers of the gripper

mining reference values for entropy and its rate of change is challenging due to their dependence on the specific object being grasped. In an ideal scenario, if slip is detected, we would want both  $V_x$  and  $V_y$  to be zero, indicating a static object. Thus, we use 0 as the reference signal for both  $V_x$  and  $V_y$ .

In the context of the book manipulation task considered in this study, which occurs solely in the  $y$ - $z$  plane, we focus on using  $V_x$  as the feature for actuation. A simple proportional control law is employed to determine the actuation. The actuation command corresponds to the change in the distance between the gripper fingers. The Robotiq Hand-E gripper accepts two inputs that can be adjusted to modify the grasp: the position between the gripper fingers and the actuation speed. Both inputs range from 0 to 255. A position command of 0 signifies the gripper being fully open, while 255 corresponds to the gripper being completely closed. The speed command of 0 indicates the slowest actuation speed, and 255 represents the highest actuation speed. In our experiments, the actuation speed is consistently set to 255 to ensure the fastest possible actuation.

The control law governing the change in finger position of the gripper is expressed as follows:

$$u = p + K_p * e \quad (4.1)$$

where  $p$  is the current position, which corresponds to the distance between the fingers of the gripper.

The flowchart below gives the flow of logic of the control algorithm:

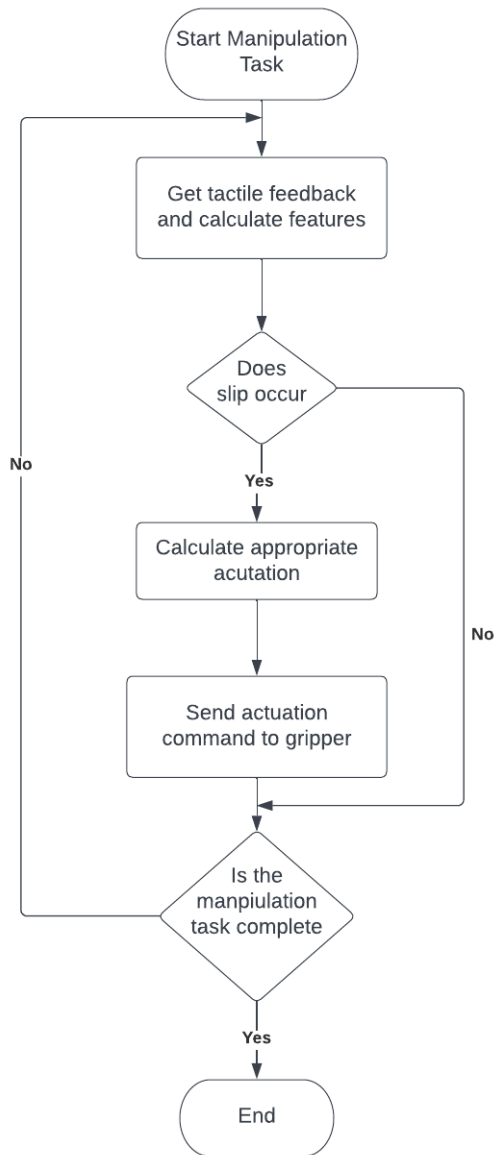


Figure 4.5: Block diagram showing the flow of logic and control during the manipulation task

To evaluate the effectiveness of this control mechanism, the same manipulation task was performed at a higher speed of 0.075 m/s. However, when using a constant incremental

decrease in the gripper finger distance upon slip detection, the grasp could not be stabilized at this increased speed. Despite slip detection, the actuation was insufficient to prevent slip from occurring. Figure 4.6 provides a visual representation of the experiment. At the beginning of the manipulation task, as shown in label 1, slip is promptly detected, resulting in an increase in the position command and a corresponding decrease in the gripper finger distance. However, in the implementation without proportional feedback control (label 2), the position command ceases to change. This indicates that the gripper has lost complete contact with the book, as the book slips out of the robot's grasp. Conversely, in the implementation with proportional feedback control, a more aggressive change in the position command is observed right from the start. As depicted in label 2, even during the ongoing manipulation task, the position command continues to increase. Once the grasp is successfully stabilized, towards the end of the manipulation task, the commanded gripper position remains constant.

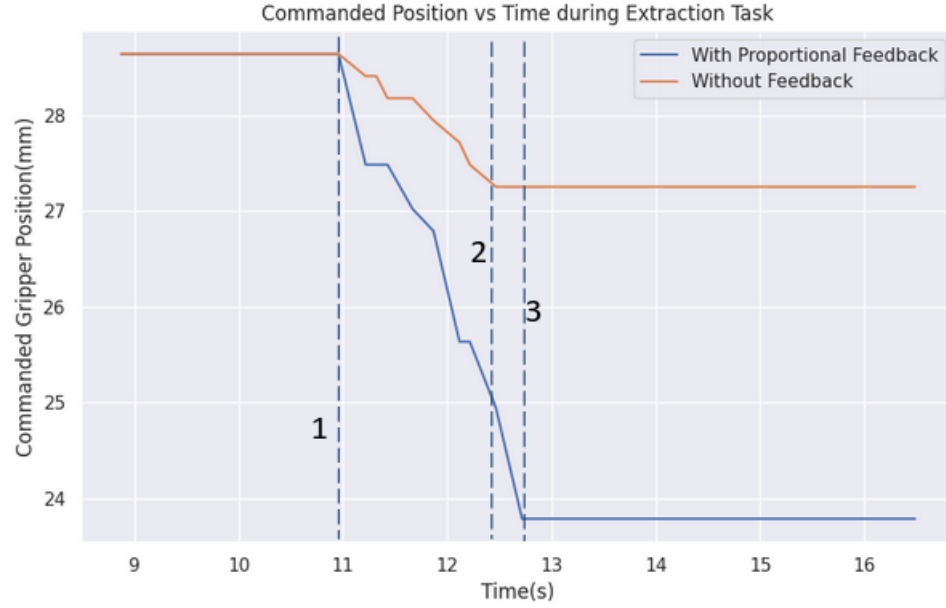


Figure 4.6: Position Command with and without Feedback Control: In the figure, the label 1 indicates the start of the manipulation task. Since the book is held with a conservative grasp, as soon as the task starts, the object starts to slip. Label 2 indicates the point where the gripper completely loses contact with the book when the robot does not have proportional feedback. And the label 3 indicates the robot having a stable grasp after proper grasp adjustment has been done using proportional feedback

Based on the results of the previous experiment, it is evident that the proposed feedback algorithm with a proportional gain can achieve a stable grasp in manipulation tasks where a simple incremental strategy falls short. To further evaluate the algorithm's performance at different manipulation speeds, an additional experiment was conducted. The objective of this experiment was to extract a book from a bookshelf, while varying the manipulation speed. Two different manipulation speeds were tested: 0.05 m/s and 0.1 m/s.

The purpose of this experiment was twofold: first, to assess the algorithm's response when the actuation speed was significantly increased, and second, to observe whether the algorithm could rapidly adjust the grasp to maintain a secure hold. Figure 4.7 illustrates the commanded position for the two different manipulation speeds, providing insights into the algorithm's performance under these conditions.

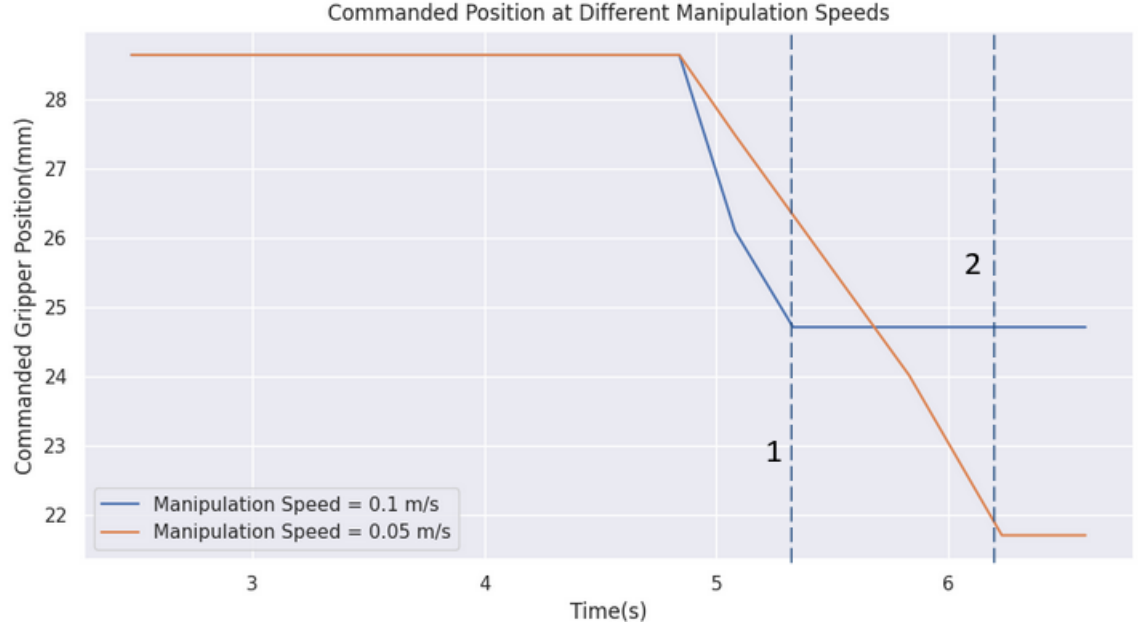


Figure 4.7: Commanded gripping position at manipulation speeds of 0.05 m/s and 0.1 m/s. 1 and 2 indicate the end of manipulation task when the speed of manipulation is 0.1 m/s and 0.05 m/s

The graph reveals several interesting observations. Similar to the previous experiments, the manipulation tasks start at the same time for both manipulation speeds. Two noteworthy observations can be made from the plot. Firstly, the commanded position exhibits a more aggressive behavior when the manipulation speed is set to 0.1 m/s, as evidenced by the steeper slope of the graph. This finding validates the choice of using  $V_x$  as the input signal for the controller and supports the hypothesis that manipulation speed correlates directly with  $V_x$ . Additionally, it can be observed that the manipulation task concludes earlier at label 1 when the speed is set to 0.1 m/s compared to the manipulation task at 0.05 m/s, which takes nearly twice as long to complete, ending at label 2. Another intriguing phenomenon observed in the graph is that, despite the slower rate of change in the commanded position during the manipulation task at 0.05 m/s, an increased number of slip instances are detected over time. Consequently, the gripper fingers close even further, resulting in a significantly smaller final position of the gripper com-

pared to the manipulation task performed at 0.1 m/s. In theory, this behavior should not occur, suggesting the possibility of false positive slip detections during the manipulation task at 0.05 m/s. This could be attributed to the fact that the classifier used for slip detection was trained solely on static data and did not involve dynamic manipulation tasks. If we look at  $V_x$  at figures 4.8 and 4.9 for both the manipulation speeds, we see that when the manipulation speed is lower, we find that  $V_x$  is higher and a lot more variation than when the manipulation speed is faster. This is quite an interesting and unusual observation, which suggests that there might be some underlying physical phenomenon which might be causing this behavior.

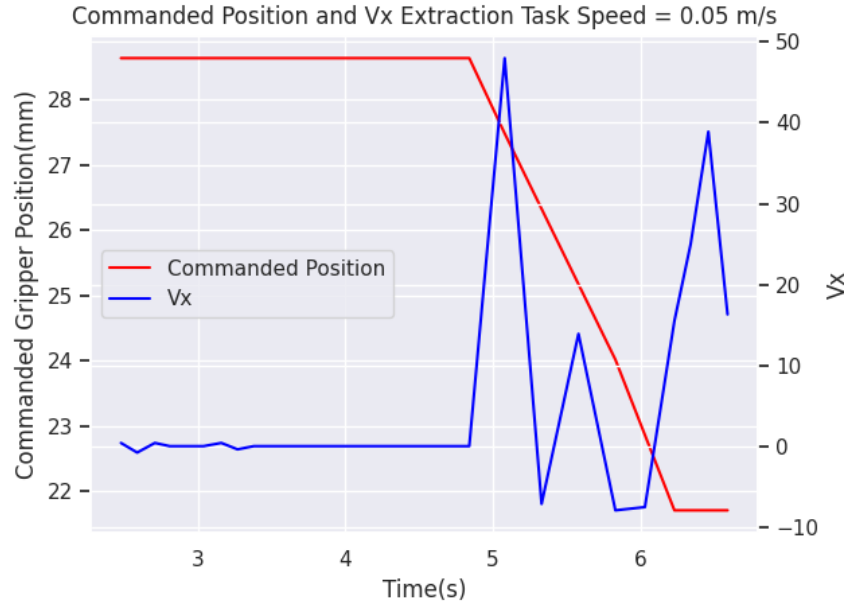


Figure 4.8: Commanded Position and  $V_x$  at manipulation speed of 0.05 m/s





Figure 4.9: Commanded Position and  $V_x$  at manipulation speed of 0.1 m/s

## Chapter 5

# CONCLUSION AND FUTURE WORK

### 5.1 Conclusion

Although there are some unexplained phenomenons, the results from the experiments show that using a tactile feedback to adaptively change the position of the gripper significantly improves speeds at which manipulation tasks can be performed at. The study also showcases a classifier which is able to detect slip across a broad range of objects and perform real-time slip detection and take actuation to prevent slip.

### 5.2 Future Work

There are some drawbacks with the current approach to slip prevention using actuation of the gripper, more work can be done in the arena to develop robust gripper actuation. Currently, the actuation strategy fails when the manipulation speed exceeds 0.1 m/s and during dynamic manipulation tasks, false positive instances of slip are detected. The feedback control also very simplistic and can be improved to make the algorithm more robust. The following sections will talk about different approaches that can be used to address this issue to develop a robust control algorithm and future work that can be done using the GelSight tactile sensors.

#### 5.2.1 Reinforcement Learning-Based Approach for Slip Prevention

One approach to develop robust control without requiring knowledge of the system dynamics is through the use of a reinforcement learning approach. In this approach, the robot learns how to pick up objects by exploring the action space. The action space consists of the speed of actuation and the change in distance between the gripper arms. A reward function can be created to heavily reward actions that minimize slip while causing minimal deformation to the grasped object. The observation space includes the features

currently used to predict slip, such as  $V_x$ ,  $V_y$ , entropy, and the rate of change of entropy. Manipulation tasks can be designed where the exact coordinates of the grasping location are known, allowing the robot to repeatedly take actions to successfully grasp the object. Gradient-free reinforcement learning methods can be highly effective for this purpose, enabling robust exploration of the solution space. However, one drawback of this approach is that reinforcement learning methods often require extensive hyper-parameter tuning and may struggle to converge to a policy for complex tasks.

### 5.2.2 CNN-Based Slip Detector with Dynamic Manipulation Training Data

The current classifier utilizes features that reduce the dimensionality of data obtained from tactile sensors. While this enables quick training of the classifiers, it does not fully utilize all the information provided by the tactile sensors. The training data used in this study only consist of instances of slip in static objects, where the object is held with a conservative grasp by the gripper without any dynamic motions performed by the robot. This can lead to false positive cases of slip detection during dynamic manipulation tasks. To address this, generating training data during dynamic motions and utilizing the entire displacement field of the markers as training data for a Convolutional Neural Network (CNN) could improve the accuracy of slip detection and avoid false positives.

### 5.2.3 Tactile Sensing for Real-Time Motion Re-Planning

The GelSight tactile sensors provide information on the marker displacement field. By correlating the marker displacement field with the relative pose of the manipulated object, real-time motion re-planning can be achieved. This capability is particularly useful for dynamic tasks such as insertion, tooling, and manipulation of objects in cluttered environments. By leveraging tactile sensing, the robot can adapt its motion in real-time based on the tactile feedback, enhancing its ability to perform complex tasks.

#### 5.2.4 *Robust Control*

In the current work, since no model of system dynamics is available, all the controller development has been done empirically. It is not feasible to develop a physics guided model of the system dynamics. Thus, a data-driven method can be tried to develop a model of the system and estimate system dynamics. This model can be used to further develop a more robust control algorithm.

## BIBLIOGRAPHY

- [1] *Following Fast-Dynamic Targets With Only Slow and Delayed Visual Feedback: A Kalman Filter and Model-Based Prediction Approach*, volume Volume 3, Rapid Fire Interactive Presentations: Advances in Control Systems; Advances in Robotics and Mechatronics; Automotive and Transportation Systems; Motion Planning and Trajectory Tracking; Soft Mechatronic Actuators and Sensors; Unmanned Ground and Aerial Vehicles of *Dynamic Systems and Control Conference*, 10 2019. V003T19A004.
- [2] Richard E. Bellman. Tactile sensing and control of robots. *IEEE Transactions on Systems, Man, and Cybernetics*, 8(6):448–452, 1978.
- [3] Lionel Birglen. Enhancing versatility and safety of industrial grippers with adaptive robotic fingers. In *2015 IEEE/RSJ International Conference on Intelligent Robots and Systems (IROS)*, pages 2911–2916, 2015.
- [4] Leo Breiman. Random forests. *Machine Learning*, 45(1):5–32, 2001.
- [5] J. Butterfass, M. Grebenstein, H. Liu, and G. Hirzinger. Dlr-hand ii: next generation of a dextrous robot hand. In *Proceedings 2001 ICRA. IEEE International Conference on Robotics and Automation*, volume 1, pages 109–114 vol.1, 2001.
- [6] Tianyi Cao, Hongbin Liu, and Haoyong Yu. Tactile sensing for robotic applications: A review. In *Proceedings of the IEEE International Conference on Robotics and Biomimetics (ROBIO)*, pages 1637–1642. IEEE, 2018.
- [7] Corinna Cortes and Vladimir Vapnik. Support-vector networks. *Machine Learning*, 20(3):273–297, 1995.
- [8] T. Cover and P. Hart. Nearest neighbor pattern classification. *IEEE Transactions on Information Theory*, 13(1):21–27, 1967.
- [9] D. R. Cox. The regression analysis of binary sequences. *Journal of the Royal Statistical Society. Series B (Methodological)*, 20(2):215–242, 1958.
- [10] Ravinder Dahiya, Giorgio Metta, Maurizio Valle, and Giulio Sandini. Tactile sensing in robotics: a review. In *Proceedings of the IEEE*, volume 98, pages 1439–1456. IEEE, 2010.

- [11] Javad Dargahi and Siamak Najarian. Review of tactile sensing technologies with applications in medical robotics. *Journal of medical engineering & technology*, 28(6):249–257, 2004.
- [12] Paolo Dario, Maria Chiara Carrozza, Mark Cutkosky, Cheng Yee Ho, and Michael W. Siegel. Tactile sensing—from humans to humanoids. *IEEE Transactions on Industrial Electronics*, 43(6):609–617, 1996.
- [13] Siyuan Dong, Daolin Ma, Elliott Donlon, and Alberto Rodriguez. Maintaining grasps within slipping bounds by monitoring incipient slip. In *2019 International Conference on Robotics and Automation (ICRA)*, pages 3818–3824, 2019.
- [14] Siyuan Dong, Wenzhen Yuan, and Edward H. Adelson. Improved gelsight tactile sensor for measuring geometry and slip. In *2017 IEEE/RSJ International Conference on Intelligent Robots and Systems (IROS)*, pages 137–144, 2017.
- [15] Pietro Griffa, Carmelo Sferrazza, and Raffaello D’Andrea. Leveraging distributed contact force measurements for slip detection: a physics-based approach enabled by a data-driven tactile sensor. In *2022 International Conference on Robotics and Automation (ICRA)*, pages 4826–4832, 2022.
- [16] R.D. Howe and M.R. Cutkosky. Sensing skin acceleration for slip and texture perception. In *Proceedings, 1989 International Conference on Robotics and Automation*, pages 145–150 vol.1, 1989.
- [17] A. Ikeda, Y. Kurita, J. Ueda, Y. Matsumoto, and T. Ogasawara. Grip force control for an elastic finger using vision-based incipient slip feedback. In *2004 IEEE/RSJ International Conference on Intelligent Robots and Systems (IROS) (IEEE Cat. No.04CH37566)*, volume 1, pages 810–815 vol.1, 2004.
- [18] Jasper Wollaston James and Nathan F. Lepora. Slip detection for grasp stabilization with a multifingered tactile robot hand. *IEEE Transactions on Robotics*, 37(2):506–519, 2021.
- [19] Jasper Wollaston James, Nicholas Pestell, and Nathan F. Lepora. Slip detection with a biomimetic tactile sensor. *IEEE Robotics and Automation Letters*, 3(4):3340–3346, 2018.
- [20] Seok Hwan Jeong, Kyung-Soo Kim, and Soohyun Kim. Designing anthropomorphic robot hand with active dual-mode twisted string actuation mechanism and tiny tension sensors. *IEEE Robotics and Automation Letters*, 2(3):1571–1578, 2017.
- [21] R.S. Johansson and G. Westling. Roles of glabrous skin receptors and sensorimotor memory in automatic control of precision grip when lifting rougher or more slippery objects. *Experimental Brain Research*, 56:550–564, 1984.

- [22] Euan Judd, Bekir Aksoy, Krishna Manaswi Digumarti, Herbert Shea, and Dario Floreano. Slip anticipation for grasping deformable objects using a soft force sensor. In *2022 IEEE/RSJ International Conference on Intelligent Robots and Systems (IROS)*, pages 10003–10008, 2022.
- [23] Kyungsup Kim, Jeehoon Park, and Sungho Choi. A review of tactile sensing technologies with applications in biomedical engineering. *Medical biology engineering & computing*, 54(2-3):165–183, 2016.
- [24] Sergey Levine, Peter Pastor, Alex Krizhevsky, and Deirdre Quillen. Learning hand-eye coordination for robotic grasping with deep learning and large-scale data collection. In *Proceedings of the IEEE International Conference on Robotics and Automation (ICRA)*, pages 3406–3413. IEEE, 2016.
- [25] Jianhua Li, Siyuan Dong, and Edward H. Adelson. Slip detection with combined tactile and visual information. *2018 IEEE International Conference on Robotics and Automation (ICRA)*, pages 7772–7777, 2018.
- [26] David G Lowe. Object recognition from local scale-invariant features. In *Proceedings of the seventh IEEE international conference on computer vision*, volume 2, pages 1150–1157. Ieee, 1999.
- [27] Alexis Maldonado, Humberto Alvarez, and Michael Beetz. Improving robot manipulation through fingertip perception. In *2012 IEEE/RSJ International Conference on Intelligent Robots and Systems*, pages 2947–2954, 2012.
- [28] Nicolás Navarro-Guerrero, Pablo Lamata, Rubén Usamentiaga, and Patricia Sanchez-Gonzalez. Haptic feedback for robot-assisted minimally invasive surgery: A review. *Frontiers in Robotics and AI*, 6:78, 2019.
- [29] Minhoon Park, Bo-Gyu Bok, Jong-Hyun Ahn, and Min-Seok Kim. Recent advances in tactile sensing technology. *Micromachines*, 9(7), 2018.
- [30] Veronica J. Santos Ravi Balasubramanian. *The Human Hand as an Inspiration for Robot Hand Development*. Springer Tracts in Advanced Robotics. Springer, New York, 2014.
- [31] Benjamin C-K Tee, Alex Chortos, Ryan R Dunn, Gregor Schwartz, Emma Eason, and Zhenan Bao. A skin-inspired tactile sensor for smart prosthetics. *Nature materials*, 14(8):831–838, 2015.
- [32] Benjamin C-K Tee, Chuan Wang, Ranulfo Allen, and Zhenan Bao. A skin-inspired organic digital mechanoreceptor. *Science*, 333(6040):830–834, 2012.

- [33] D. Tsetserukou, R. Tadakuma, H. Kajimoto, and S. Tachi. Optical torque sensors for implementation of local impedance control of the arm of humanoid robot. In *Proceedings 2006 IEEE International Conference on Robotics and Automation.*, pages 1674–1679, 2006.
- [34] Filipe Veiga, Benoni Edin, and Jan Peters. Grip stabilization through independent finger tactile feedback control. *Sensors*, 20(6), 2020.
- [35] Filipe Veiga, Herke van Hoof, Jan Peters, and Tucker Hermans. Stabilizing novel objects by learning to predict tactile slip. In *2015 IEEE/RSJ International Conference on Intelligent Robots and Systems (IROS)*, pages 5065–5072, 2015.
- [36] Benjamin Ward-Cherrier, Nicholas Pestell, Luke Cramphorn, Benjamin Winstone, Maria Elena Giannaccini, Jonathan Rossiter, and Nathan F. Lepora. The tactip family: Soft optical tactile sensors with 3d-printed biomimetic morphologies. *Soft Robotics*, 5(2):216–227, 2018. PMID: 29297773.
- [37] Nicholas Wettels, Veronica Santos, Roland Johansson, and Gerald Loeb. Biomimetic tactile sensor array. *Advanced Robotics*, 22:829–849, 08 2008.
- [38] Ziwei Xia, Zhen Deng, Bin Fang, Yiyong Yang, and Fuchun Sun. A review on sensory perception for dexterous robotic manipulation. *International Journal of Advanced Robotic Systems*, 19(2), MAR 2022.
- [39] H. Xiao and X. Chen. Robotic target following with slow and delayed visual feedback. *International Journal of Intelligent Robotics and Applications*, 4(4):378–389, 2020.
- [40] Hui Xiao, Yaakov Bar-Shalom, and Xu Chen. A collaborative sensing and model-based real-time recovery of fast data flows from sparse measurements. *IEEE Transactions on Industrial Electronics*, 67(8):6806–6814, 2020.
- [41] S. Wang Y. She, A. Rodriguez S. Dong, N. Sunil, and E. Adelson. Cable manipulation with a tactile-reactive gripper. In *Robotics: Science and Systems (RSS)*, 2020.
- [42] Wenzhen Yuan, Siyuan Dong, and Edward H. Adelson. Gelsight: High-resolution robot tactile sensors for estimating geometry and force. *Sensors*, 17(12), 2017.
- [43] Wenzhen Yuan, Rui Li, Mandayam A. Srinivasan, and Edward H. Adelson. Measurement of shear and slip with a gelsight tactile sensor. In *2015 IEEE International Conference on Robotics and Automation (ICRA)*, pages 304–311, 2015.



## Appendix A

**TRAINING AND TESTING DATA**

<https://drive.google.com/drive/folders/1T1U10F4AUxZtBMev2VRmZOfXw1Vzc1Do?usp=sharing>

## Appendix B

**ADDITIONAL PLOTS WITH  $V_x$  AND COMMANDED GRIPPER POSITION FOR DIFFERENT MANIPULATION SPEEDS**

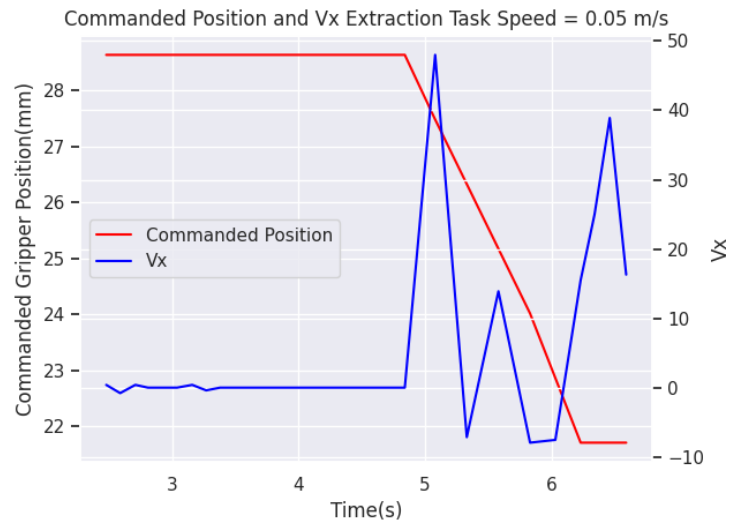


Figure B.1: Commanded Position and  $V_x$  at manipulation speed of 0.05 m/s



Figure B.2: Commanded Position and  $V_x$  at manipulation speed of 0.1 m/s

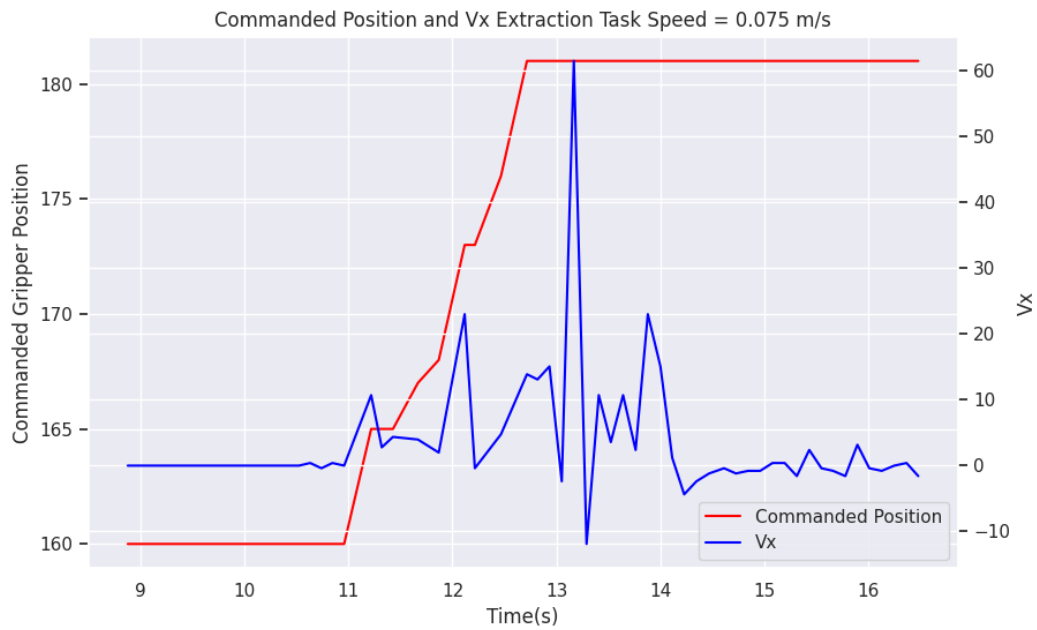


Figure B.3: Commanded Position and  $V_x$  at manipulation speed of 0.075 m/s